Sustainable Energy & Fuels

Interdisciplinary research for the development of sustainable energy technologies

Accepted Manuscript

This article can be cited before page numbers have been issued, to do this please use: W. Schmitt, S. Tandon, J. Soriano-Lopez, A. C. Kathalikkattil, G. Jin, P. Wix, M. Venkatesan, R. Lundy, M. A. Morris and G. W. Watson, *Sustainable Energy Fuels*, 2020, DOI: 10.1039/D0SE00701C.

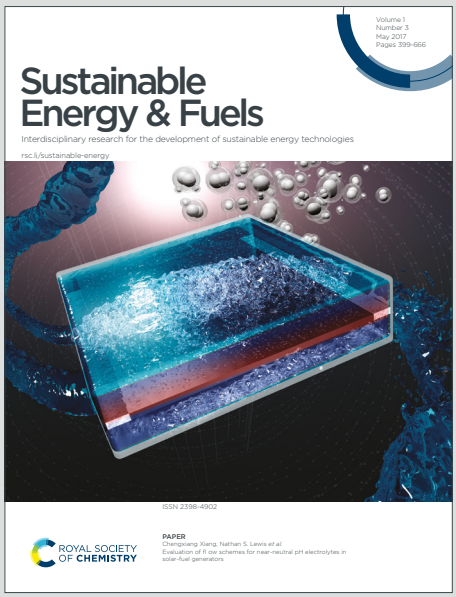

ROYAL SOCIETY OF CHEMISTRY

rsc.li/sustainable-energy

View Article Online
DOI: 10.1039/D0SE00701C

COMMUNICATION

A cubane-type manganese complex with H_2O oxidation capabilities

Received 00th January 20xx,
Accepted 00th January 20xx

DOI: 10.1039/x0xx00000x

Swetanshu Tandon,[a,b] Joaquín Soriano-López,[a,b] Amal C. Kathalikkattil,[a,b] Guanghua Jin,[a,b] Paul Wix,[a,b] Munuswamy Venkatesan,[c] Ross Lundy,[a,b] Michael A. Morris,[a,b] Graeme W. Watson,[a]* and Wolfgang Schmitt*[a,b]

We report the synthesis and characterisation of $[Mn_8K_2O_4(OH)_2((CH_3)_3CCOO)_{16}]$ whose cluster core shares some features with the oxygen evolving complex (OEC), the natural water oxidation catalyst. Importantly, this complex provides a bio-inspired complex that promotes catalytic H_2O oxidation at neutral pH value.

Ever increasing energy demands and the closely related issue of global warming derived from fossil fuel combustion have enforced the development of renewable energy sources as one of the most important scientific challenges today.[1] Solar energy, among other energy sources like wind and hydropower, is considered to be more ecologically sustainable and of higher economic impact due to its ubiquity. However, the implementation of solar energy as an alternative, sustainable energy source requires storage concepts as its supply is generally irregular both in terms of time and location. Nature stores energy in chemical form involving the breakage and formation of chemical bonds in the presence of sunlight. H_2O is the obvious candidate for energy storage due to its abundance, and solar energy can be used to split water photochemically or electrochemically to obtain H_2 which can then be used as a potentially carbon-free fuel with high gravimetric energy capacity.[2] Electrochemically, H_2O splitting occurs at 1.23 V (vs. reversible hydrogen electrode, RHE) via the reactions shown in Scheme 1.[3]

Energetically, the bottleneck is associated with the oxidation half-reaction which occurs in green plants in photosystem-II (PS-II), as part of photosynthesis.[2, 4] Numerous successful attempts towards crystallising PS-II have greatly aided our understanding of its complex structure.[5] The oxygen evolving complex (OEC)

$$2H_2O \longrightarrow O_2 + 4H^+ + 4e^- \qquad E_{anodic} = 1.23 \text{ V vs. RHE}$$
$$4H^+ + 4e^- \longrightarrow 2H_2 \qquad E_{cathodic} = 0 \text{ V vs. RHE}$$
$$2H_2O \longrightarrow 2H_2 + O_2 \qquad E_{total} = 1.23 \text{ V}$$

Scheme 1 Redox reaction and half-reactions of the water splitting process.

represents the active site for water oxidation in PS-II. It comprises of a distorted $\{Mn_3Ca\}$ cubane unit that has a dangling Mn atom attached to it. The OEC resides in its $\{Mn^{III}_2Mn^{IV}_2\}$ form, which is commonly referred to as the dark stable S_1 state.[6] During photosynthesis, the complex undergoes structural changes cycling through different intermediate (S_2, S_3 and S_4) states, each of which differs from the other in the number of charge equivalents stored. The release of O_2 is accompanied by the formation of the $\{Mn^{III}_3Mn^{IV}\}$ S_0 state which transforms back to the S_1 state.[6a, 7] This half-reaction occurs at neutral pH conditions[8] under which the majority of the synthetic catalyst fail to achieve satisfactory activity.[9] The harsh oxidising conditions damage the OEC and deactivate it during H_2O oxidation within approximately 30 minutes[10] but owing to self-healing mechanisms, it reconstitutes to catalyse H_2O oxidation for extended periods.[11]

Over the last decades, considerable efforts have been dedicated to the synthesis of $\{Mn_4\}$ cubanes that mimic the OEC.[12] However, the incorporation of a hetero-metal atom into the cubane unit has been found to be synthetically difficult and only a few such cubane complexes have been reported.[13] A notable example among these, is a $\{Mn_4Ca\}$ complex[13d, 13f] which is structurally similar to the distorted cubane unit of the OEC and which is the only $\{Mn_3Ca\}$ cubane system known to incorporate a dangling Mn centre. However, catalytic H_2O oxidation has not been reported for this distorted, mixed-metal cubane complex. We have been interested in the electronic and magnetic attributes of Mn coordination clusters[14] whereby our recent efforts were directed towards developing reactive OEC mimics with cubane type motifs. To this end, we have modified the synthesis of a $\{Mn_6\}$ complex[15] to form the complex $[Mn_8K_2(\mu_3\text{-}O)_4(\mu\text{-}OH)_2((CH_3)_3CCOO)_{16}(CH_3CN)_2]\cdot CHCl_3$ (**Mn_8K_2**) which

[a] School of Chemistry & CRANN Institute, University of Dublin, Trinity College, Dublin 2, Ireland.
[b] AMBER Centre, University of Dublin, Trinity College, Dublin 2, Ireland.
[c] School of Physics & CRANN Institute, University of Dublin, Trinity College, Dublin 2, Ireland.
Email: watsong@tcd.ie, schmittw@tcd.ie

† Electronic Supplementary Information (ESI) available: Experimental and computational details, Fig. S1-S14 and Tables S1-S7. See DOI: 10.1039/x0xx00000x

reveals some noteworthy similarities to the OEC. Importantly, we demonstrate its catalytic activity towards H_2O oxidation at neutral pH value, thus, providing an example of a hetero-metallic system that captures the structural attributes of the OEC and can promote the oxidation of H_2O.

Structural Characterisation

Single crystals of **Mn_8K_2** form upon refluxing $KMnO_4$ in the presence of pivalic acid in CH_3CN, followed by addition of $CHCl_3$ and they were characterised using single crystal X-ray diffraction (Table S1, ESI). This synthetic protocol exploits the structure directing effects of the pivalate ligands modifying established synthetic routes to Mn oxo-clusters with butterfly motifs[15] to assemble a polynuclear complex with cubane-type arrangement.

Mn_8K_2 crystallises in the monoclinic crystal system in the space group $P2_1/n$ and contains an octanuclear Mn complex in which all the Mn centres adopt octahedral coordination environments. The structure can be regarded as a dimer of two distorted {Mn_4K} cubane units that are symmetry related by an inversion centre, and that are bridged by pivalate ligands and two μ_3-oxo groups, O2 and its symmetry equivalent (**Fig. 1**(a)). Each {Mn_4K} cubane unit consists of three Mn^{III} ions, Mn1, Mn2 and Mn3, and a K^+ ion. The fourth Mn^{III} centre, Mn4, structurally relates to the dangling Mn centre of the OEC and is linked to {Mn_4K} through an oxo-ligand, O1, and the O-donors of four pivalate ligands. Altogether, each {Mn_4K} motif is stabilised by nine pivalate ligands whose O-donors occupy the tetragonally elongated Mn^{III} Jahn-Teller sites. Two μ_3-oxo ligands, O1 and O2, and a μ_2-hydroxo O-donor, O3 form three of the vertices of the cubane unit. The latter is further engaged in a H-bond involving a monodentate pivalate ligand that binds to Mn3 (O-O donor–acceptor distance *ca.* 2.6 Å). Within each of the {Mn_4K} units, the K^+ ions are strongly incorporated into the cluster core and are connected to all four Mn^{III} centres *via* μ_3-oxo and pivalate moieties, thus distinguishing **Mn_8K_2** from other Mn coordination complexes that employ K^+ ions merely as charge-balancing counterions.

The molecular structure of **Mn_8K_2** is particularly distinctive as it shares some geometrical features with the OEC as highlighted in **Fig. 1**(b) and (c). Considering the +III oxidation states of the Mn centres which were unambiguously assigned by bond valance sum analysis and DFT calculations (tables S2 and S3), **Mn_8K_2** may be compared to the formally reduced S_{-1} state of the OEC.[16]

Some Mn-O distances in the cubane unit, in general, compare well with those found in OEC whereby differences result from ligand restrains and the reduced nature of the Mn^{III} centres and their characteristic bonding features. The K-O bond distances are, on average, approximately 0.3 Å longer in comparison to the Ca-O bond distances in OEC. Most significant differences to the OEC structure are associated with the Mn3-K/Ca distance and the atom position and connectivity of the dangling Mn4 centre which, in the OEC, is additionally bound to Mn1 *via* an oxo-ligand.

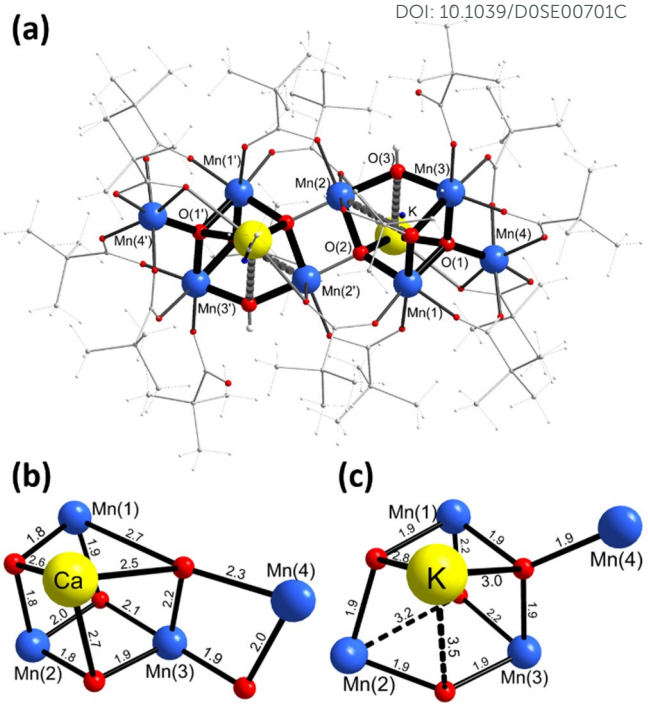

Fig. 1 (**a**) Crystal structure of **Mn_8K_2**. (**b**) and (**c**) Comparison of the core of the cubane-type complex in OEC and **Mn_8K_2**, respectively (interatomic distances are given in Å). Weaker inter-atomic distances >3 Å are represented as intersected lines. Colour code: Mn (blue), K/Ca (yellow), C (grey), N (blue), O (red) and H (light grey).

The phase purity and thermal stability of the compound were determined using powder X-ray diffraction and thermogravimetric analysis, respectively (Fig. S1 and S2, ESI). The magnetic susceptibility data reveals dominant antiferromagnetic interactions between the Mn centres in **Mn_8K_2** leading to an $S = 0$ ground spin state (Fig. S3, ESI). These observations are supported by the computational DFT analyses (Tables S5 - S7, ESI) performed using the methods described in ref. 17.

Electrochemical Analysis

The outlined structural features and the characteristics that relate to the reduced form of OEC prompted us to investigate the electrochemical properties of the complex and to characterise its ability to undergo oxidation and influence the electrochemical H_2O oxidation. Prior to these studies, the hydrolytic stability of **Mn_8K_2** was investigated. For this purpose, **Mn_8K_2** was dispersed in Millipore water by sonication for 30 minutes after which the residual material was collected, washed and then dried at room temperature (**Mn_8K_2***). Energy dispersive X-ray spectroscopy (EDX) measurements clearly confirm that the sample transforms upon sonication in aqueous systems giving rise to a black-brown, amorphous solid (Fig. S4, ESI) with a Mn:K ratio >20:1, rather than 4:1, as observed for **Mn_8K_2**. Additionally, the Mn:O ratio in **Mn_8K_2*** was found to be ~1:3 and no residual carbon content was detected. The inherent instability of the molecular structure of **Mn_8K_2** upon sonication

in aqueous solution is further supported by changes observed in the infrared (IR) and X-ray photoelectron spectroscopy (XPS) data of **Mn_8K_2*** compared to **Mn_8K_2** (Fig. S5 and S6, ESI). The XPS data suggests that **Mn_8K_2** transforms into manganese-derived oxides.[18] The K^+ ions, on the other hand, and oligonuclear Mn pivalate complexes are released into the aqueous solution phase upon sonication as demonstrated by mass spectrometry giving rise to signals corresponding to monomeric and dimeric manganese pivalate species (Fig. S7, ESI). The low solubility of **Mn_8K_2** in water, but moreover its instability when forced to dissolve in water, renders it unsuitable for homogeneous electrochemical studies in aqueous medium. Previously conducted electrocatalytic H_2O oxidation experiments using a polymorph of **Mn_8K_2** thus, only serve to characterise the activity of the hydrolytic decomposition products.[13e]

To investigate the electrochemical properties of **Mn_8K_2** in aqueous medium, modified carbon paste electrodes were prepared by dispersing **Mn_8K_2** in commercial carbon paste (**Mn_8K_2/CP**). These carbon paste based electrodes are known to provide a hydrophobic environment and have previously been applied to stabilise molecular species, preventing rapid hydrolytic decomposition even under very acidic conditions.[19] Cyclic voltammetry (CV) of **Mn_8K_2/CP** electrodes in potassium phosphate buffer at pH 7.2 (KP*i*, 50 mM) using KNO_3 (1 M) as electrolyte, results in a strong catalytic wave due to H_2O oxidation (**Fig. 2**(a)). The similarity in the first and the fifth CV cycle indicates that there is no observable transformation of **Mn_8K_2** during this period.

To study the kinetic profile of this H_2O oxidation reaction, linear sweep voltammetry (LSV) was performed using a **Mn_8K_2/CP** rotating disk electrode at a low scan rate of 1 mV/s to ensure quasi-steady state conditions during the experiment. The **Mn_8K_2** catalyst loading was varied between 10 and 40 wt-% of the total **CP** blend. From the electrochemical profile (**Fig. 2**(b) and (c)), it is evident that higher **Mn_8K_2** loadings significantly increase the current densities and decrease the onset potential of the H_2O oxidation reaction. Above a catalyst loading of 40 wt-%, the electrodes become brittle and unsuitable for obtaining reproducible data and thus 40 wt-% **Mn_8K_2/CP** loadings were employed in further experiments.

40 wt-% **Mn_8K_2/CP** electrodes, give rise to an onset overpotential of 420 mV for the H_2O oxidation reaction and a Tafel slope of 255 mV dec^{-1} (**Fig. 2**(c) and (d)) within an overpotential range of 400-700 mV (Table 1). Similar Tafel slopes have previously been observed for other H_2O oxidation catalysts.[20] Within the 700-800 mV range, the slope was found to be slightly higher (280 mV dec^{-1}). Tafel analysis for successive linear sweep scans using these **Mn_8K_2/CP** electrodes, resulted in characteristic slope changes (Fig. S9, ESI). Upon cycling, the Tafel slope above 700 mV decreases to ~230 mV dec^{-1} and a new redox peak at *ca.* ~1.1 V (*vs* NHE) is observed after 5 linear sweep cycles. The appearance of a new peak and the convolution behaviour suggests that **Mn_8K_2** is catalytically active operating at an onset potential of 420 mV and then undergoes transformation to a new species which is catalytically active above 700 mV.

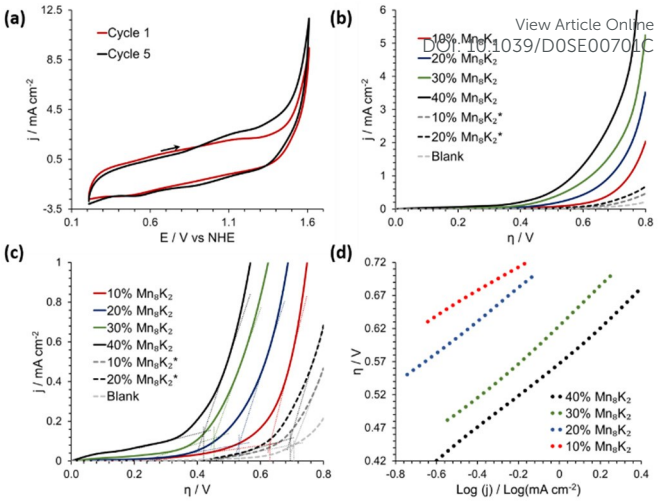

Fig. 2 (**a**) Cyclic voltammograms for **Mn_8K_2/CP** (40 wt-% loading) in a KP*i* buffer solution at pH 7.2. The sudden rise in the current density with increasing potential is characteristic of catalytic water oxidation. (**b**) Linear sweep voltammograms for **Mn_8K_2/CP** and **Mn_8K_2*/CP** at different loadings. (**c**) The determined onset potentials for **Mn_8K_2/CP** and **Mn_8K_2*/CP** at various loadings. (**d**) Steady-state Tafel data for **Mn_8K_2/CP** electrodes for various catalyst loadings.

To substantiate this hypothesis, linear sweep voltammetry experiments were conducted using **Mn_8K_2*/CP** electrodes (**Fig. 2**(b) and (c)). In this case, however, the **Mn_8K_2*** content was restricted to 20 wt-% as electrodes became brittle at higher loadings. The electrochemical behaviour of **Mn_8K_2*** bears close similarity with that observed at the later stages of the successive linear sweep experiments using **Mn_8K_2/CP** electrodes thereby suggesting that **Mn_8K_2** transforms to a species that exhibits a similar electrochemical behaviour as **Mn_8K_2*** while facilitating H_2O oxidation. Indeed, the XPS data suggests that both materials are structurally similar but differ in the protonation state of the O donor atoms (Fig. S6, ESI). This difference is not surprising as the different experimental conditions of the hydrolytic transformations are expected to result in variable quantities of coordinating O^{2-}, OH^- and H_2O species.

The onset overpotential was found to be 695 mV for a 20 wt-% **Mn_8K_2*** loading in contrast to 532 mV for the corresponding **Mn_8K_2/CP** electrode. Thus, the electrochemical data of **Mn_8K_2*** corresponds to that previously reported for a polymorph of **Mn_8K_2** for which the activity has been attributed to Mn_2O_3.[13e] To confirm the formation of oxides under these conditions,

Table 1 The onset overpotential for water oxidation with Mn_8K_2/CP and Mn_8K_2*/CP electrodes at different loadings in the overpotential range of 400-700 mV. The onset potential is clearly lower for Mn_8K_2/CP electrodes.

Loading	Onset overpotential (mV)	Tafel slope (mV dec^{-1})
10% Mn_8K_2/CP	630	190
20% Mn_8K_2/CP	532	245
30% Mn_8K_2/CP	453	278
40% Mn_8K_2/CP	420	255
10% Mn_8K_2*/CP	706	195
20% Mn_8K_2*/CP	695	250

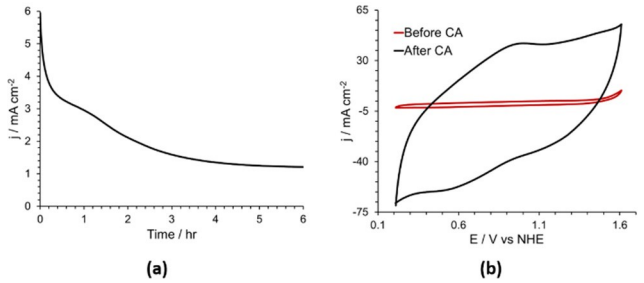

Fig. 3 (**a**) CA data for **Mn_8K_2/CP** (40 wt-% loading) at 1.56 V *vs* NHE in KP*i* buffer solution at pH 7.2 for the first six hours. (**b**) Cyclic voltammograms for **Mn_8K_2/CP** before and after CA.

chronoamperometry (CA) at an applied potential of 1.56 V (vs NHE) was performed for 16 hours using a **Mn_8K_2/CP** working electrode (**Fig. 3**(a) and Fig. S10, ESI). Cyclic voltammetry (**Fig. 3**(b)) after CA revealed a new oxidation peak at *ca.* ~1.02 V (vs NHE). The appearance of this new signal[21] and the XPS analysis (Fig. S6, ESI) confirm that the decomposed material comprises of defective Mn oxides.[18]

These results demonstrate that **Mn_8K_2** is indeed active towards water oxidation and with time, transforms to a less-active material that displays a similar structural and electrochemical behaviour as **Mn_8K_2***. Just like the OEC, **Mn_8K_2** decomposes rapidly, but it appears to be highly active for H_2O oxidation in comparison to the corresponding oxide phase. This can be inferred from a comparison of the linear sweep voltammograms of **Mn_8K_2** and **Mn_8K_2*** at 10 and 20 wt-% loading (**Fig. 2**(b) and (c)) which show that **Mn_8K_2** is highly active even though the concentration of Mn centres and hence, the number of active sites per unit weight, is much lower for **Mn_8K_2** in comparison to **Mn_8K_2***.

As the CV and LSV experiments confirm that the activity is derived from **Mn_8K_2**, we decided to obtain some mechanistic insights. The catalytic behaviour of **Mn_8K_2** can only be be facilitated by the voids along the crystallographic *c*-axis which are characterised by a cross-sectional diameter of 5.20 and where constitutional $CHCl_3$ molecules reside. Preliminary DFT calculations suggest that the substitution of the monodentate pivalate group bound to Mn3 with an OH^- ion is energetically feasible rendering Mn3 as a possible initiation site for catalysis (ESI). Further investigations will be required to elucidate the mechanistic details for the H_2O oxidation reaction which might reveal some insights into the OER activity of the OEC.

To conclude, we have demonstrated that a synthetic, heterometallic {Mn_4}-based cubane structure that bears some structural features to the natural OEC, can promote the catalytic oxidation of H_2O. The complex can be synthesised using inexpensive commercial chemicals and the synthesis highlights the structural directing role of pivalate groups allowing the synthesis of cubane-type Mn clusters. Modification of the alkyl moieties of the carboxylates may provide a path for further structural modification to obtain structurally more accurate OEC mimics.

To stabilise the molecular species and to investigate its electrocatalytic behaviour, **Mn_8K_2** was dispersed in a protective carbon paste matrix. Electrodes with a 40 wt-% **Mn_8K_2** loading, give rise to an onset overpotential of 420 mV and a Tafel slope of 255 mV dec^{-1} at pH = 7.2. Similar to the OEC, **Mn_8K_2** shows relatively high catalytic activity and also undergoes decomposition under oxidative, hydrolytic conditions to form a less-active species.

View Article Online DOI: 10.1039/D0SE00701C

Conflicts of interest

There are no conflicts to declare.

Acknowledgements

The authors thank the Irish Research Council (GOIPG/2015/2952), Science Foundation Ireland (SFI 13IA/1896), the European Research Council (CoG 2014-647719) and the Horizon 2020 Marie Sklodowska-Curie programme (agreement No. 713567) for funding. ICHEC is acknowledged for computational resources.

Notes and references

1 N. S. Lewis and D. G. Nocera, *Proc. Natl. Acad. Sci. USA*, 2006, **103**, 15729-15735.
2 A. J. Bard and M. A. Fox, *Acc. Chem. Res.*, 1995, **28**, 141-145.
3 B. M. Hunter, H. B. Gray and A. M. Muller, *Chem. Rev.*, 2016, **116**, 14120-14136.
4 (a) J. P. McEvoy and G. W. Brudvig, *Chem. Rev.*, 2006, **106**, 4455-4483; (b) H. Dau and I. Zaharieva, *Acc. Chem. Res.*, 2009, **42**, 1861-1870; (c) J. Yano and V. Yachandra, *Chem. Rev.*, 2014, **114**, 4175-4205; (d) M. Perez-Navarro, F. Neese, W. Lubitz, D. A. Pantazis and N. Cox, *Curr. Opin. Chem. Biol.*, 2016, **31**, 113-119.
5 (a) K. N. Ferreira, T. M. Iverson, K. Maghlaoui, J. Barber and S. Iwata, *Science*, 2004, **303**, 1831-1838; (b) Y. Umena, K. Kawakami, J. R. Shen and N. Kamiya, *Nature*, 2011, **473**, 55-60; (c) M. Suga, F. Akita, K. Hirata, G. Ueno, H. Murakami, Y. Nakajima, T. Shimizu, K. Yamashita, M. Yamamoto, H. Ago and J. R. Shen, *Nature*, 2015, **517**, 99-103.
6 (a) H. Dau and M. Haumann, *Coord. Chem. Rev.*, 2008, **252**, 273-295; (b) V. Krewald, M. Retegan, N. Cox, J. Messinger, W. Lubitz, S. DeBeer, F. Neese and D. A. Pantazis, *Chem. Sci,*, 2015, **6**, 1676-1695.
7 B. Kok, B. Forbush and M. Mcgloin, *Photochem. Photobiol.*, 1970, **11**, 457-475.
8 (a) J. G. Metz, P. J. Nixon, M. Rogner, G. W. Brudvig and B. A. Diner, *Biochemistry*, 1989, **28**, 6960-6969; (b) I. Vass and S. Styring, *Biochemistry*, 1991, **30**, 830-839; (c) K. G. V. Havelius and S. Styring, *Biochemistry*, 2007, **46**, 7865-7874.
9 (a) T. Takashima, K. Hashimoto and R. Nakamura, *J. Am. Chem. Soc.*, 2012, **134**, 1519-1527; (b) F. Jiao and H. Frei, *Energy Environ. Sci.*, 2010, **3**, 1018-1027.
10 A. Zavafer, M. H. Cheah, W. Hillier, W. S. Chow and S. Takahashi, *Sci. Rep.*, 2015, **5**.
11 S. V. Baranov, G. M. Ananyev, V. V. Klimov and G. C. Dismukes, *Biochemistry*, 2000, **39**, 6060-6065.
12 (a) M. Yagi, K. V. Wolf, P. J. Baesjou, S. L. Bernasek and G. C. Dismukes, *Angew. Chem. Int. Ed.*, 2001, **40**, 2925-2928; (b) R. Brimblecombe, G. F. Swiegers, G. C. Dismukes and L. Spiccia, *Angew. Chem. Int. Ed.*, 2008, **47**, 7335-7338; (c) R. Brimblecombe, A. Koo, G. C. Dismukes, G. F. Swiegers and L. Spiccia, *J. Am. Chem. Soc.*, 2010, **132**, 2892-2894; (d) Y. L. Gao, R. H. Crabtree and G. W. Brudvig, *Inorg. Chem.*, 2012, **51**, 4043-4050; (e) R. Al-Oweini, A. Sartorel, B. S. Bassil, M.

View Article Online
DOI: 10.1039/D0SE00701C

Natali, S. Berardi, F. Scandola, U. Kortz and M. Bonchio, *Angew. Chem. Int. Ed.*, 2014, **53**, 11182-11185; (f) B. Schwarz, J. Forster, M. K. Goetz, D. Yucel, C. Berger, T. Jacob and C. Streb, *Angew. Chem. Int. Ed.*, 2016, **55**, 6329-6333; (g) G. Maayan, N. Gluz and G. Christou, *Nat. Catal.*, 2018, **1**, 48-54; (h) T. Ghosh and G. Maayan, *Angew. Chem. Int. Ed.*, 2019, **58**, 2785-2790.

13 (a) J. S. Kanady, E. Y. Tsui, M. W. Day and T. Agapie, *Science*, 2011, **333**, 733-736; (b) S. Mukherjee, J. A. Stull, J. Yano, T. C. Stamatatos, K. Pringouri, T. A. Stich, K. A. Abboud, R. D. Britt, V. K. Yachandra and G. Christou, *Proc. Natl. Acad. Sci. USA*, 2012, **109**, 2257-2262; (c) J. S. Kanady, P. H. Lin, K. M. Carsch, R. J. Nielsen, M. K. Takase, W. A. Goddard and T. Agapie, *J. Am. Chem. Soc.*, 2014, **136**, 14373-14376; (d) C. X. Zhang, C. H. Chen, H. X. Dong, J. R. Shen, H. Dau and J. Q. Zhao, *Science*, 2015, **348**, 690-693; (e) Y. Mousazade, M. R. Mohammadi, P. Chernev, R. Bikas, R. Bagheri, Z. L. Song, T. Lis, H. Dau and M. M. Najafpour, *Catal. Sci. Technol.*, 2018, **8**, 4390-4398; (f) C. Chen, Y. Chen, R. Yao, Y. Li and C. Zhang, *Angew. Chem. Int. Ed.*, 2019, **58**, 3939-3942.

14 (a) L. Zhang, R. Clérac, P. Heijboer and W. Schmitt, *Angew. Chem. Int. Ed.*, 2012, **51**, 3007-3011; (b) L. Zhang, T. Chimamkpam, C. I. Onet, N. Y. Zhu, R. Clérac and W. Schmitt, *Dalton Trans.*, 2016, **45**, 17705-17713.

15 M. Poyraz, M. Sari, S. Cevik and O. Buyukgungor, *Acta Cryst. E*, 2006, **62**, M1442-M1444.

16 D. Koulougliotis, *Photosynthetica*, 2009, **47**, 567-574.

17 S. Tandon, M. Venkatesan, W. Schmitt and G. W. Watson, *Dalton Trans.*, 2020, DOI: 10.1039/D0DT01404D.

18 M. C. Biesinger, B. P. Payne, A. P. Grosvenor, L. W. M. Lau, A. R. Gerson and R. S. Smart, *Appl. Surf. Sci.*, 2011, **257**, 2717-2730.

19 M. Blasco-Ahicart, J. Soriano-Lopez, J. J. Carbo, J. M. Poblet and J. R. Galan-Mascaros, *Nat. Chem.*, 2018, **10**, 24-30.

20 (a) M. H. Miles, E. A. Klaus, B. P. Gunn, J. R. Locker and W. E. Serafin, *Electrochim. Acta*, 1978, **23**, 521-526; (b) H. J. Shi and G. H. Zhao, *J. Phys. Chem. C*, 2014, **118**, 25939-25946.

21 M. M. Najafpour, N. J. Moghaddam, S. M. Hosseini, S. Madadkhani, M. Holynska, S. Mehrabani, R. Bagheri and Z. L. Song, *Catal. Sci. Technol.*, 2017, **7**, 3499-3510.

Graphical Abstract:

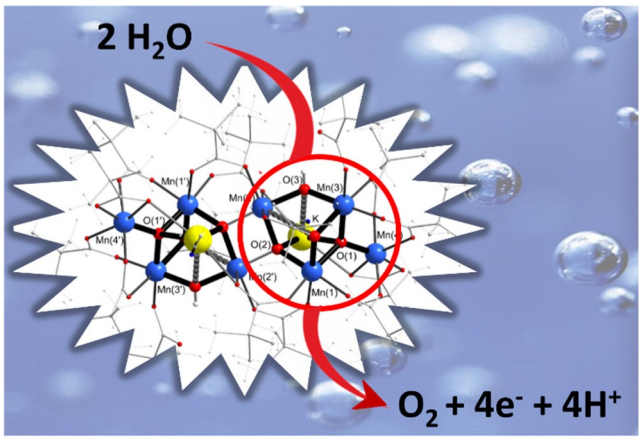

A Mn coordination cluster whose core shares some features with the natural oxygen evolving complex provides a bio-inspired complex that promotes catalytic H_2O oxidation at neutral pH value.